

Search for Vector-Like Singlet Top (T) Quark in a Future Muon-Proton (μp) Collider at $\sqrt{s} = 5.29, 6.48$, and 9.16 TeV using Advanced Machine Learning Architectures

Haroon Sagheer,¹ M. Tayyab Javaid,² Mudassar Hussain,³ M. Danial Farooq,² Ijaz Ahmed,^{2,*} and Jamil Muhammad^{4,†}

¹*Riphah International University, Islamabad*

²*Federal Urdu University of Arts, Science and Technology, Islamabad, Pakistan*

³*Riphah International University, Faisalabad*

⁴*Sang-Ho College & Department of Physics,
Konkuk University, Seoul 05029, South Korea*

(Dated: February 3, 2026)

Abstract

In this work, we explore the discovery potential of Vector-Like Singlet Top quarks (T) at a future μp collider with center-of-mass energies of 5.29, 6.48, and 9.16 TeV, providing a unique environment to probe beyond Standard Model limits. We analyze the $T \rightarrow Wb$ decay mode in both fully hadronic (bjj) and leptonic ($bl\nu$) final states, offering a multi-channel assessment of T -quark sensitivity across a mass range of 2 to 5 TeV. Our methodology employs multivariate classifiers such as Boosted Decision Trees (BDTs) and Multi-Layer Perceptrons (MLP) to optimize signal-to-background discrimination in complex final states. The results demonstrate that the 9.16 TeV benchmark acts as a definitive discovery machine; even with 100 fb^{-1} of data, the statistical significance exceeds 5σ up to 4 TeV masses. We identify a crossover effect where hadronic channels provide superior reach at intermediate masses due to higher branching ratios, while leptonic channels offer robustness at 5 TeV where purity limits detection. Incorporating a 20% systematic uncertainty via Asimov significance (Z_A), we quantify the transition from fluctuation-dominated to systematic-dominated regimes at high luminosities. At 3000 fb^{-1} , regions with $g^* \in [0.20, 0.50]$ and m_T up to 4 TeV are discoverable via the hadronic channel with MLP, and regions with $g^* \in [0.10, 0.50]$ and m_T up to 5 TeV are accessible through the leptonic channel with BDT, highlighting the collider's potential to probe new physics beyond the Standard Model.

PACS numbers: 12.60.Fr, 14.65.Jk, 12.60.-i, 14.80.Fd

Keywords: Vector-Like Quarks, Muon-Proton Collider, Multivariate Analysis, Machine Learning, Signal Significance.

*Electronic address: ijaz.ahmed@fuuast.edu.pk

†Electronic address: mjamil@konkuk.ac.kr

I. INTRODUCTION

The Standard Model (SM) of particle physics has achieved remarkable success in explaining a wide array of experimental results, culminating in the landmark discovery of the Higgs boson at the Large Hadron Collider (LHC) [12, 13]. Despite this, the SM is widely regarded as an effective theory that leaves fundamental questions unanswered, particularly regarding the gauge hierarchy problem, the origin of the flavor structure, and the nature of dark matter [14–16]. Vector-like quarks (VLQs) emerge as a natural and compelling extension in numerous Beyond the Standard Model (BSM) frameworks designed to address these deficiencies, including composite Higgs models, little Higgs constructions, extra-dimensional scenarios, and superstring-inspired E6 models [1, 4–7]. Unlike chiral quarks, VLQs are defined by the fact that their left- and right-handed components transform identically under the SM $SU(2)_L \times U(1)_Y$ gauge group, allowing for gauge-invariant mass terms that are not strictly tied to the electroweak symmetry breaking scale [22, 23, 25].

In many of these theoretical setups, such as the Randall-Sundrum models [4] or the $SO(5)/SO(4)$ composite Higgs framework [17, 18], the top-partner T quark with electric charge $+2/3$ plays a critical role in stabilizing the Higgs mass by canceling quadratic divergences stemming from top-quark loops [19–21]. The phenomenology of these partners is primarily dictated by their mixing with third-generation SM quarks via Yukawa interactions, as detailed in effective descriptions of quark mixing [3, 8, 24]. At high-energy colliders, a heavy top partner T is expected to decay into a third-generation quark and a SM boson (Wb , tZ , and tH), with the branching fractions for the tZ and tH modes becoming nearly comparable at high masses due to the Goldstone boson equivalence theorem [8, 26, 27].

Experimental searches for VLQs are a major priority for the ATLAS and CMS collaborations, which have established lower mass limits approaching 1.3–1.5 TeV for various VLQ species [30, 57]. While pair production of VLQs is a largely model-independent process mediated by the strong force [31, 33], single production through electroweak interactions probes the specific mixing parameters of the model and often provides a broader discovery reach at high mass scales due to its lower kinematic threshold [26, 28]. However, as the mass of the top partner increases into the multi-TeV regime, its decay products become significantly boosted, resulting in highly collimated jet topologies. These “fat jets” present a substantial challenge for standard jet reconstruction and traditional cut-based analysis techniques, necessitating the development of more sophisticated identification strategies [40, 41].

To extend the reach for VLQ discovery, the physics community is investigating future facilities

beyond the High-Luminosity LHC. While lepton colliders like CLIC provide a clean environment for precision measurements [2], the proposed muon–proton (μp) collider offers a unique synergy by combining the high energy of a proton beam with the precision of a muon probe, effectively reducing multi-jet backgrounds while maintaining a higher center-of-mass energy than typical e^+e^- machines [21, 33]. In this study, we focus on the single production of vector-like T quarks at three specific center-of-mass energies: $\sqrt{s_{\mu p}} = 5.29, 6.48$, and 9.16 TeV, analyzing both fully hadronic and leptonic decay channels [1].

To maximize the discovery potential in these high-energy environments, we employ advanced Multivariate Analysis (MVA) techniques. Traditional cut-based selections often struggle to capture the complex, non-linear correlations between kinematic variables in highly boosted final states. By utilizing the Toolkit for Multivariate Data Analysis (TMVA) [34], we implement classifiers such as Boosted Decision Trees (BDTs), Multilayer Perceptrons (MLP), and Likelihood [35, 54]. These approaches, rooted in foundational machine learning algorithms [37–39], significantly improve signal extraction and background rejection, allowing us to quantify the discovery reach across a broad range of benchmark mass points and luminosities.

This paper focuses on single production of a vector-like top quark at a future muon–proton collider. We study three center-of-mass energies, $\sqrt{s_{\mu p}} = 5.29, 6.48$, and 9.16 TeV, and analyze both fully hadronic and leptonic decays [1]. Lepton colliders such as CLIC provide a complementary, cleaner environment for VLQ searches and serve as a useful reference point [2]. The goal is to map the kinematic structure of the signal, quantify the discovery reach, and compare a clean cut-based selection with multivariate classifiers in a consistent, data-driven way. The theoretical setup is summarized in Sec. II, while the analysis strategy and benchmarks are given in Sec. III.

II. A BRIEF OVERVIEW OF VECTOR-LIKE SINGLET TOP QUARK MODEL

A. Field Content and Mixing

Vector-like quarks can be arranged as $SU(2)_L$ singlets, doublets, or triplets. In the singlet case relevant for this study, the top partner T carries electric charge $+2/3$ and can mix with SM up-type quarks through Yukawa couplings to the Higgs doublet. Because VLQ mass terms are gauge invariant, a bare mass M_T is allowed, and electroweak symmetry breaking induces additional mixing between T and the SM sector [1]. This mixing opens up the electroweak decay modes that dominate the collider phenomenology.

B. Effective Interactions

Following a standard effective parametrization for singlet VLQs [1, 2], the interactions of a single T quark with electroweak gauge bosons can be written in a compact, model-independent form as

$$\mathcal{L}_T = \frac{g}{\sqrt{2}} \kappa_W V_{4i} \bar{T}_{L/R} \gamma^\mu W_\mu^+ d_{iL/R} + \frac{g}{2c_W} \kappa_Z V_{4i} \bar{T}_{L/R} \gamma^\mu Z_\mu u_{iL/R} - \frac{\kappa_H V_{4i} M_T}{v} \bar{T}_{R/L} H u_{iL/R} + \text{h.c.} \quad (1)$$

Here V_{4i} denotes the mixing between the heavy state and the SM generation i , $\kappa_{W,Z,H}$ encode the coupling strengths to the W , Z , and Higgs bosons, v is the electroweak vacuum expectation value, and $c_W = \cos \theta_W$. This parametrization is consistent with the standard VLQ framework and makes it straightforward to relate collider observables to the underlying mixing pattern.

C. Branching Ratios

For the decay $T \rightarrow V q_i$ with $V = W, Z, H$, the branching fractions can be expressed as follows [8]:

$$\text{BR}(T \rightarrow V q_i) = \frac{\kappa_V^2 |V_{4i}|^2 \Gamma_V^0}{\sum_{j=1}^3 |V_{4j}|^2 \sum_{V'=W,Z,H} \kappa_{V'}^2 \Gamma_{V'}^0}, \quad (2)$$

where Γ_V^0 denotes the partial width in the limit of unit coupling. In practice, the $T \rightarrow Wb$ channel is dominant for the benchmark scenarios considered here, while the tZ and tH modes are smaller but nearly equal at high mass, in line with the Goldstone equivalence expectation.

III. EVENT SELECTIONS AND KINEMATICS DISTRIBUTIONS

A. Hadronic Section

The search for a Vector-Like Top (VLT) quark singlet (T) in the fully hadronic channel at a muon-proton collider presents a complex experimental environment. The signal process, $\mu^- p \rightarrow \nu_\mu T \bar{b} \rightarrow \nu_\mu (Wb) \bar{b} \rightarrow \nu_\mu (jjb) \bar{b}$, results in a final state composed of at least four hard partons and significant missing transverse energy (\mathbb{E}_T^{miss}) from the recoil neutrino. Moreover, highly dominating Standard Model backgrounds are following:

- SM Single Top: $\mu^- p \rightarrow \nu_\mu t \bar{b} \rightarrow \nu_\mu (W^+ b) \bar{b} \rightarrow \nu_\mu (jjb) \bar{b}$
- $W + \text{jets}$: $\mu^- p \rightarrow \nu_\mu W^+ j \rightarrow \nu_\mu (jj) j$

- $Z + \text{jets}$: $\mu^- p \rightarrow \nu_\mu Z j \rightarrow \nu_\mu (jj) j$
- Multijet: $\mu^- p \rightarrow \nu_\mu jj$

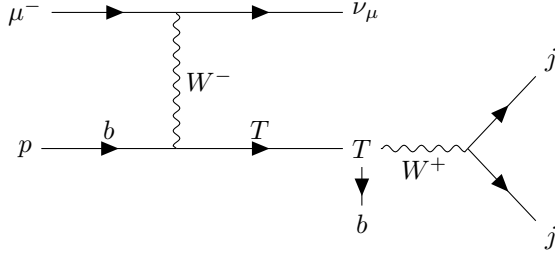


FIG. 1: Representative leading-order (LO) Feynman diagram for the single production of a vector-like singlet top quark in the hadronic channel at a μp collider: $\mu^- p \rightarrow \nu_\mu T b$, followed by $T \rightarrow W^+ b$ and $W^+ \rightarrow jj$.

The dataset is simulated using MadGraph5 [59] , PYTHIA 8.3 [60] was utilized for hadronization and parton showering. Later, we implemented the detector effects using Delphes 3.5 [61]. To isolate this multi-TeV resonance from Standard Model (SM) backgrounds, we employ a sequential selection strategy utilizing 9 specific kinematic observables. However, a detailed explanation is articulated for the motivation behind the selection criteria as below:

- **Object Acceptance and Trigger Thresholds:** Initial event selection ensures that all physics objects fall within the detector's optimal tracking and calorimetric volume. We impose a global geometric constraint on all reconstructed jets, requiring $|\eta| < 2.5$. This phenomenally reduces the noise in the standard model backgrounds as well as cleans the signal, as it can be seen in the evolution of signal efficiencies across the tables at $\sqrt{s} = 5.29, 6.48$, and 9.16 TeV. To trigger on the hard scattering expected from a heavy resonance, we define stringent thresholds for the leading and sub-leading jets:
- **Leading Jet Kinematics ($p_T^{j_1}, \eta_{j_1}$):** We require $p_T^{j_1} > 120$ GeV. This threshold is critical for triggering on the energetic decay products of the VLT.
- **Sub-leading Jet Kinematics ($p_T^{j_2}, \eta_{j_2}$):** A secondary threshold of $p_T^{j_2} > 50$ GeV is applied. For high-mass signals, these two leading jets typically originate from the boosted W or T decay chain.

TABLE I: A Distribution of the Cumulative Signal Efficiencies for Hadronic Channel across all m_T (2000-5000 GeV) points at $\sqrt{s} = 5.29$ TeV.

Selection Cuts	2000 GeV	2500 GeV	3000 GeV	3500 GeV	4000 GeV	4500 GeV	5000 GeV
$ \eta_j < 2.5$	0.50068	0.49836	0.49784	0.50288	0.49940	0.50016	0.49928
$p_T^{j_1} > 120$ GeV	0.49532	0.49472	0.49508	0.50088	0.49808	0.49872	0.49828
$p_T^{j_2} > 50$ GeV	0.49084	0.48988	0.48824	0.49092	0.48456	0.48232	0.47168
$N_{\text{jets}} \geq 4$	0.17828	0.16952	0.16064	0.15420	0.14428	0.13532	0.09748
$N_{b\text{jets}} \geq 2$	0.05388	0.04720	0.03932	0.03288	0.02980	0.02548	0.01600
$H_T > 450$ GeV	0.05376	0.04712	0.03924	0.03288	0.02968	0.02548	0.01600
$E_T^{\text{miss}} > 10$ GeV	0.05316	0.04640	0.03888	0.03276	0.02948	0.02532	0.01596
$\epsilon\%$	5.316	4.640	3.888	3.276	2.948	2.532	1.596

TABLE II: Distribution of the Cumulative Signal Efficiencies for Hadronic Channel across all m_T (2000-5000 GeV) points at $\sqrt{s} = 6.48$ TeV.

Selection Cuts	2000 GeV	2500 GeV	3000 GeV	3500 GeV	4000 GeV	4500 GeV	5000 GeV
$ \eta_j < 2.5$	0.49824	0.50124	0.49580	0.50088	0.49932	0.49820	0.50312
$p_T^{j_1} > 120$ GeV	0.49452	0.49832	0.49380	0.49912	0.49760	0.49688	0.50220
$p_T^{j_2} > 50$ GeV	0.49204	0.49548	0.49076	0.49480	0.49176	0.49008	0.49416
$N_{\text{jets}} \geq 4$	0.21268	0.20432	0.20016	0.19080	0.18812	0.18152	0.17756
$N_{b\text{jets}} \geq 2$	0.06548	0.05868	0.05248	0.04640	0.03952	0.03696	0.03236
$H_T > 450$ GeV	0.06488	0.05860	0.05240	0.04636	0.03952	0.03696	0.03236
$E_T^{\text{miss}} > 10$ GeV	0.06412	0.05804	0.05164	0.04600	0.03916	0.03680	0.03220
$\epsilon\%$	6.412	5.408	4.848	4.304	3.720	3.512	3.068

To distinguish the massive signal from soft SM backgrounds, discriminating variables such as global energy and multiplicity are analyzed along with several crucial variables for the multivariate training using advanced machine learning methods.

- **Energy Scales (H_T , E_T^{miss}):** We utilize the scalar sum of all jet transverse momenta, $H_T = \sum |p_{T,jet}|$, with a minimum requirement of $H_T > 450$ GeV. Additionally, we require $E_T^{\text{miss}} > 10$ GeV to ensure the presence of the recoil neutrino.
- **Multiplicities ($N_{\text{jets}}, N_{b\text{-jets}}$):** We mandate $N_{\text{jets}} \geq 4$ and $N_{b\text{-jets}} \geq 2$. The heavy-flavor requirement is the primary veto against light-flavor W/Z production and SM multijet noise.

The associated production of the Vector-Like Top with a bottom quark results in a final state with multiple b -jets. The kinematics of the two leading b -jets ($p_T^{b_1}, \eta_{b_1}, p_T^{b_2}, \eta_{b_2}$) are critical for separation. Furthermore, we exploit:

- **Angular Separation (ΔR_{bb}):** as the VLT mass increases, its boost leads to more collimated decay products, shifting the ΔR_{bb} distribution toward lower values compared to non-resonant backgrounds.
- **Reconstructed Mass (M_{bjj}):** The central resonant observable, exhibiting a Jacobian peak at the T mass. The reconstruction of the VLT candidate is achieved through a global χ^2 minimization fit. This procedure yields several high-impact variables for our multivariate analysis. The algorithm iterates through jet permutations to find the most likely $W \rightarrow jj$ and $T \rightarrow Wb$ candidates by minimizing:

$$\chi^2 = \frac{(M_{jj} - M_W)^2}{\sigma_W^2} + \frac{(M_{jjb} - M_{top})^2}{\sigma_{top}^2} \quad (3)$$

- **Reconstructed Top p_T (p_T^T):** Captures the extreme boost of the VLT candidate, which is significantly higher than that of SM single-top or $t\bar{t}$ production.

TABLE III: Distribution of the Cumulative Signal Efficiencies for Hadronic Channel across all m_T (2000-5000 GeV) points at $\sqrt{s} = 9.16$ TeV.

Selection Cuts	2000 GeV	2500 GeV	3000 GeV	3500 GeV	4000 GeV	4500 GeV	5000 GeV
$ \eta_j < 2.5$	0.49976	0.50416	0.49884	0.50292	0.49784	0.49768	0.50296
$p_T^{j_1} > 120$ GeV	0.49656	0.50168	0.49704	0.50060	0.49608	0.49616	0.50100
$p_T^{j_2} > 50$ GeV	0.49276	0.49876	0.49448	0.49896	0.49428	0.49436	0.49944
$N_{\text{jets}} \geq 4$	0.25232	0.25824	0.24812	0.25188	0.24996	0.23784	0.24324
$N_{b\text{jets}} \geq 2$	0.08516	0.07564	0.06688	0.05968	0.05884	0.05088	0.04876
$H_T > 450$ GeV	0.08476	0.07532	0.06672	0.05964	0.05884	0.05080	0.04876
$E_T^{\text{miss}} > 10$ GeV	0.07848	0.07084	0.06284	0.05680	0.05512	0.04836	0.04632
$\epsilon\%$	7.848	7.084	6.284	5.680	5.512	4.836	4.632

As detailed in the signal efficiency tables, the reconstruction efficiency is strongly energy-dependent. At $\sqrt{s} = 9.16$ TeV, the cumulative efficiency for a 5000 GeV VLT reaches 4.632% after all reconstruction validations, a three-fold increase over the 5.29 TeV energy run. This demonstrates the enhanced discovery potential at higher center-of-mass energies, where the signal products are more easily separated from the SM background tail.

B. Leptonic Section

The search for a Vector-Like Singlet Top (T) Quark at a muon-proton collider in a leptonic final state utilizes the signal: $\mu^- p \rightarrow \nu_\mu T \bar{b} \rightarrow \nu_\mu (W b) \bar{b} \rightarrow \nu_\mu (\ell \nu b) \bar{b}$ that involves a final state with a single lepton, multiple neutrinos, and heavy-flavor jets, and standard model backgrounds of Single Top and W +jets given as: $\mu^- p \rightarrow \nu_\mu t \bar{b} \rightarrow \nu_\mu (W^+ b) \bar{b} \rightarrow \nu_\mu (\ell^+ \nu_\ell b) \bar{b}$ and $\mu^- p \rightarrow \nu_\mu W^+ j \rightarrow \nu_\mu (\ell^+ \nu_\ell) j$ respectively. The data samples were simulated using MadGraph5 [10] followed by an integrated parton showering via PYTHIA 8.3 [9]. Later, the detector effects were applied using DELPHES 3.5 [11]. To isolate the multi-TeV signal, a sequential selection strategy is implemented and described in detail. The impact of each cut on the signal efficiencies across the three center-of-mass energies ($\sqrt{s} = 5.29, 6.48$, and 9.16 TeV) is detailed in the Tables VII.

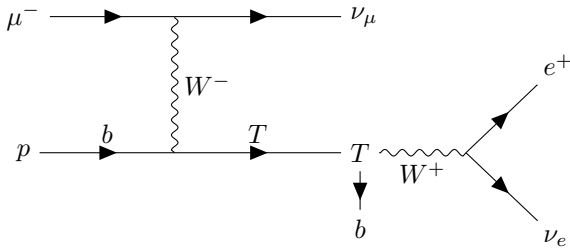


FIG. 2: Representative leading-order (LO) Feynman diagram for single production of a vector-like singlet top quark in the leptonic channel at a μp collider: $\mu^- p \rightarrow \nu_\mu T b$, followed by $T \rightarrow W^+ b$ and $W^+ \rightarrow e^+ \nu_e$.

- **Lepton Acceptance and $p_T^\ell > 150$ GeV:** The initial requirements for an isolated lepton ($|\eta| < 2.4$) maintain an efficiency of $\sim 35 - 37\%$. The p_T threshold of 150 GeV is specifically designed to suppress the soft leptonic tail from Background 2. Interestingly, the efficiency of the p_T cut increases with M_T ; for instance, at 5.29 TeV, efficiency rises from 32.2% for $M_T = 2000$ GeV to 34.8% for $M_T = 5000$ GeV. Physically, as the VLT mass increases, its decay products are naturally more energetic, allowing a higher fraction to surpass the hard trigger threshold.
- **Jet Multiplicity and B-Tagging:** We mandate $N_{jets} \geq 2$ ($p_T > 30$ GeV) and exactly one b -tagged jet ($p_T > 80$ GeV). This stage represents the most significant efficiency "tax." At $\sqrt{s} = 9.16$ TeV, the efficiency drops from $\sim 28\%$ to $\sim 10\%$ for a 4000 GeV mass. This drop is due to the extreme Lorentz boost of the T quark; as its products become collimated, the b -jet often merges with the lepton or neutrinos, or fails the isolation criteria for high-mass

resonances.

- **Missing Energy ($MET > 80$ GeV):** Since the signal production vertex and W decay both involve neutrinos, MET is a crucial discriminator. The efficiency remains stable across mass points ($\sim 9 - 10\%$ cumulative)[cite: 14, 17], effectively filtering out QCD events with instrumental MET .
- **Angular Collimation ($\Delta R(\ell, b) > 1.5$):** This cut is the primary veto for the SM single-top background. As VLT mass increases, the efficiency for this cut consistently decreases—dropping from 9.97% to 7.26% at 6.48 TeV. This trend is a signature of the “boosted” regime where decay products are forced into a narrow cone, a physical effect more pronounced at higher masses.

TABLE IV: Tabular Representation of the Cumulative Signal Efficiencies for Leptonic Channel across all mass points of m_T at $\sqrt{s} = 5.29$ TeV.

Selection Cuts	2000 (GeV)	2500 (GeV)	3000 (GeV)	3500 (GeV)	4000 (GeV)	4500 (GeV)	5000 (GeV)
$N_\ell \geq 1$ ($P_T > 10$)	0.37504	0.37572	0.36992	0.36660	0.36452	0.36688	0.36156
$\eta_\ell < 2.4$	0.37460	0.37524	0.36964	0.36628	0.36408	0.36648	0.36092
$p_T^\ell > 150$ GeV	0.32204	0.33828	0.34156	0.34408	0.34656	0.35172	0.34860
$N_{jets} \geq 2$ ($p_T > 30$ GeV)	0.23708	0.24880	0.25024	0.24572	0.24600	0.23456	0.17488
$b_{jet} \equiv 1$ ($P_T > 80$)	0.10820	0.10576	0.09420	0.08796	0.08452	0.07280	0.04544
MET > 80 GeV	0.09628	0.09752	0.08816	0.08248	0.07960	0.06840	0.04308
$\Delta R(\ell, b) > 1.5$	0.09180	0.09320	0.08332	0.07828	0.07532	0.06432	0.04248
$\epsilon\%$	9.180	9.320	8.332	7.828	7.532	6.432	4.248

TABLE V: Tabular Representation of the Cumulative Signal Efficiencies for Leptonic Channel across all mass points of m_T at $\sqrt{s} = 6.48$ TeV.

Selection Cuts	2000 (GeV)	2500 (GeV)	3000 (GeV)	3500 (GeV)	4000 (GeV)	4500 (GeV)	5000 (GeV)
$N_\ell \geq 1$ ($P_T > 10$)	0.37292	0.36832	0.36876	0.36696	0.35872	0.36312	0.36208
$\eta_\ell < 2.4$	0.37204	0.36768	0.36820	0.36664	0.35864	0.36260	0.36156
$p_T^\ell > 150$ GeV	0.32404	0.33244	0.34112	0.34648	0.34392	0.34876	0.34900
$N_{jets} \geq 2$ ($p_T > 30$ GeV)	0.25128	0.26008	0.26572	0.26648	0.26324	0.26296	0.25860
$b_{jet} \equiv 1$ ($P_T > 80$)	0.11496	0.10888	0.10296	0.09768	0.09128	0.08680	0.08092
MET > 80 GeV	0.10408	0.10088	0.09552	0.09184	0.08664	0.08228	0.07708
$\Delta R(\ell, b) > 1.5$	0.09972	0.09696	0.09064	0.08716	0.08096	0.07692	0.07260
$\epsilon\%$	9.972	9.696	9.064	8.716	8.096	7.692	7.260

TABLE VI: Tabular Representation of the Cumulative Signal Efficiencies for Leptonic Channel across all mass points of m_T at $\sqrt{s} = 9.16$ TeV.

Selection Cuts	2000 (GeV)	2500 (GeV)	3000 (GeV)	3500 (GeV)	4000 (GeV)	4500 (GeV)	5000 (GeV)
$N_\ell \geq 1$ ($P_T > 10$)	0.35056	0.35216	0.35600	0.35132	0.35616	0.35552	0.35368
$\eta_\ell < 2.4$	0.34880	0.35052	0.35488	0.35020	0.35528	0.35468	0.35292
$p_T^\ell > 150$ GeV	0.30532	0.32152	0.33252	0.33240	0.34040	0.34264	0.34228
$N_{jets} \geq 2$ ($p_T > 30$ GeV)	0.24812	0.26388	0.27676	0.27504	0.27980	0.28236	0.27692
$b_{jet} \equiv 1$ ($P_T > 80$)	0.11176	0.11188	0.10968	0.10152	0.09968	0.09936	0.09284
MET > 80 GeV	0.10196	0.10328	0.10316	0.09660	0.09472	0.09452	0.08940
$\Delta R(\ell, b) > 1.5$	0.09732	0.09724	0.09736	0.09024	0.08796	0.08820	0.08268
$\epsilon\%$	9.732	9.724	9.736	9.024	8.796	8.820	8.268

The multivariate analysis utilizes highly sophisticated 8 variables to separate the signal from SM noise. In particular:

- **Reconstructed Mass ($M_{b\ell\nu}$):** This is the primary resonant variable. By solving for the neutrino p_z using the W -mass constraint, we reconstruct the parent VLT mass. Signal events peak at M_T , while non-resonant W +jets events form a broad continuum, allowing the MVA to achieve high separation.
- **Transverse Mass ($M_T(\ell, MET)$):** For the W +jets background, this variable is bounded by the W -mass Jacobian peak (~ 80 GeV). Since the W in our signal originates from a multi-TeV T decay, its transverse mass extends significantly higher, providing a clean separation boundary.
- **Helicity Angle ($\cos\theta^*$):** This angular observable probes the polarization of the W boson. Because the VLT singlet model involves a different chiral coupling than the SM top, the $\cos\theta^*$ distribution provides a unique shape that the MVA uses to veto SM top events. Therefore, it is a help discriminant when the shapes of signal and backgrounds are observed by multivariate analysis. It can be calculated using:

$$\cos\theta^* = \frac{\vec{p}_\ell^* \cdot \vec{p}_W}{|\vec{p}_\ell^*||\vec{p}_W|} \quad (4)$$

- **p_T Ratio and MET:** The ratio of lepton p_T to MET or jet p_T measures the kinematic balance of the system. In VLT decays, the products follow a specific energy-sharing profile, whereas in $W + j$ events, the jet p_T is often asymmetric relative to the lepton, making the ratio a powerful discriminant.

The signal efficiencies are taken together and displayed in Fig. 3. We observe that the leptonic mode provides a cleaner outreach and critical cross-check which adds to the total discovery potential of the future muon-proton collider [40, 57].

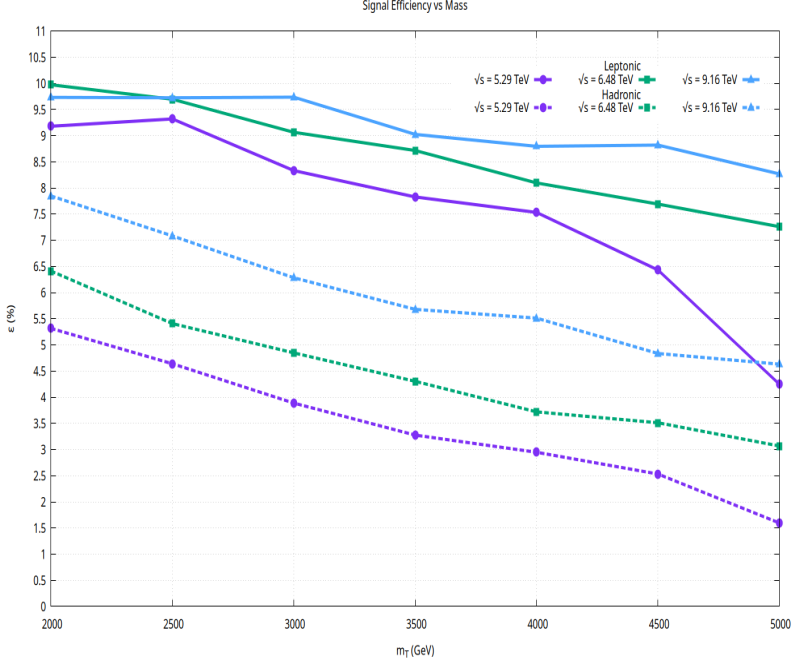


FIG. 3: The Hadronic and Leptonic Signal efficiency $\epsilon(\%)$ versus m_T evaluated at the collider energies of $\sqrt{s} = 5.29, 6.48$, and 9.16 TeV. It can be observed that the efficiency monotonically decreases for both channels at higher mass points. It is clear that the signature of Leptonic Signal is relatively clear across all collider energies; whereas, the Hadronic channel gets high jet signatures at higher center of mass energy due to jet substructure algorithm.

IV. ADVANCED MACHINE LEARNING TECHNIQUES FOR THE FEASIBILITY STUDY

A. Signal Extraction Through Multivariate Analysis

To classify and separate signal events from the background ensemble, we utilize 4 major machine learning classifiers : Boosted Decision Trees (BDT), Gradient Boosted Decision Trees (BDTG), Multilayer Perceptrons (MLP), and Likelihood. These ML Models are implemented via the “Toolkit for Multivariate Data Analysis (TMVA)” [34]. Multivariate techniques offer a significant advantage over traditional cut-based methods, as they are capable of capturing high-dimensional and non-

linear correlations between kinematic variables that are otherwise lost in sequential classification by rectangular cuts.

TMVA classifiers such as BDTs employ a tree-based architecture typically consisting of several hundred individual decision trees. In this study, we utilize the “AdaBoost” and “GradBoost” algorithms to iteratively assign higher weights to misclassified events, thereby improving the separation power in regions where signal and background distributions overlap significantly.

Similarly, the Multilayer Perceptron (MLP) is an Artificial Neural Network (ANN) characterized by a multi-layered architecture consisting of input, hidden, and output layers. Each neuron in the hidden layer performs a non-linear transformation of the physical variables using an “Activation Function” (such as Sigmoid or ReLU). This process allows the network to check for complex correlations and model the underlying patterns in the ensemble distribution. After successful training, the MLP provides a distribution score between 0 and 1, facilitating a visual and statistical classification between signal and background.

The Likelihood classifier is a simpler approach compared to BDTs and MLP, as it operates on the “Naive Bayes” assumption that input variables are independent. This method constructs probability density functions (PDFs) by generating histograms for signal (f_s) and background (f_B) for each variable. In this setup, the signal and background likelihoods are built as:

$$L_s(x) = \prod_{i=1}^n f_{s,i}(x_i), \quad L_B(x) = \prod_{i=1}^n f_{B,i}(x_i) \quad (5)$$

Finally, the projected likelihood computes the likelihood ratio, which serves as the final discriminant:

$$y_{LH}(x) = \frac{L_s(x)}{L_s(x) + L_B(x)} \quad (6)$$

The resulting distribution scores for both the Likelihood and the tree-based classifiers are presented between -1 and 1 . It is most important to note that “Projected Likelihood” was observed to be underperformed because the training variables are highly correlated. It does not mean that the ML model is over-trained; however, Likelihood is used as benchmark to reveal the correlation between the variables computationally.

All classifiers are trained using a set of input variables for both the hadronic and leptonic channels that provide the most separation power and discrimination between signal and background events. These variables include kinematic properties of the reconstructed objects, and b-tagging information. The features that are used as inputs to classifiers are listed in Table VII.

The events from signal and background are split into two subsets: one subset is employed for the training process, while the other serves as a test sample for cross validation and to monitor

TABLE VII: The Complete Set of Discriminating Input Variables for the Classification Task for ML-based Architectures for both Leptonic and Hadronic Datasets at $\sqrt{s} = 5.29, 6.48$, and 9.16 TeV

Distribution of Input Variables			
Leptonic	Description	Hadronic	Description
$M_{b\ell\nu}$	Reconstructed Mass of Vector-Like Top Quark	E_T^{miss}	Missing Transverse Energy
ρ_{Tl}^{\pm}	Transverse Momenta of Leptons	H_T	Sum of Transverse Momenta of all the jets ($\sum p_{T,jet} $)
$\Delta R(\ell, b)$	Angular Correlation of Leptons and b-tagged jets	$\Delta R_{b_{j1}, b_{j2}}$	Angular Separation between leading and sub-leading b-tagged jets
ρ_{Tbjet}	Transverse Momenta of b-tagged jets	M_{bjj}	Reconstructed Mass of Vector-Like Top Quark
$\cos \theta^*$	Helicity Angle of decayed Products (l, W)	ρ_{T^T}	Transverse Momentum of Vector-like Top Quark
E_T^{miss}	Missing Transverse Energy	ρ_{Tj1}	Transverse Momentum of Leading jet
$M_T(\ell, MET)$	Transverse Mass of W-Boson	ρ_{Tj2}	Transverse Momentum of sub-leading jet
$\frac{p_T^\ell}{p_T^b}$	Ratio of transverse momenta of leptons and b-jets	ρ_{Tbjet1}	Transverse Momentum of Leading b-tagged jet
		ρ_{Tbjet2}	Transverse Momentum of sub-leading b-tagged jet

against over-training by conducting the “Kolmogorov-Smirnov (KS) Test”. In addition to that, the KS test is an important feature which shows that how ML classifiers are generalizing well over the given datasets. This non-parametric test computes the cumulative frequency distribution functions (CDFs) while having training and testing sample in view. Overall, it checks if both come from the same statistical distribution or validates the statistical consistency between the distribution with minor statistical fluctuations. The test statistic is given below:

$$D_{n,m} = \sup_x |F_{1,n}(x) - F_{2,n}(x)| \quad (7)$$

This is carried out by calculating the p value which in the experimental particle physics regime has to be greater than 0.05 ($p > 0.05$). Otherwise, the classifier is declared over-trained, which means it would start to memorize the underlying patterns in the ensemble distribution. The over-training evaluation of all the classifiers for both Hadronic in Fig 4 and in Fig 5 for Leptonic analysis section.

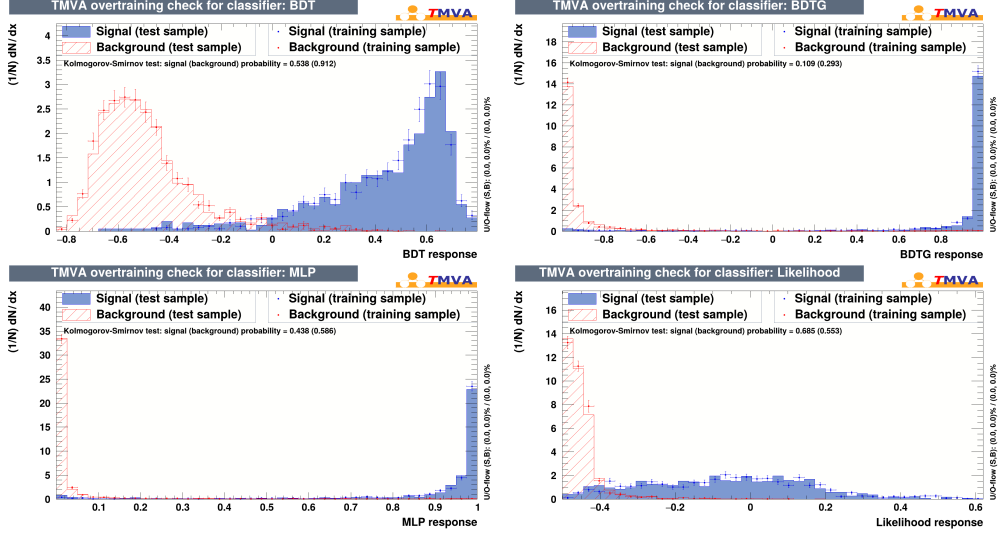


FIG. 4: The Output Distribution Score and Overtraining Evaluation of all ML Classifiers (BDTs, MLP, Likelihood) for Hadronic Analysis after Multivariate Training conducted at $\sqrt{s} = 9.16\text{TeV}$ for $m_T = 3000\text{GeV}$.

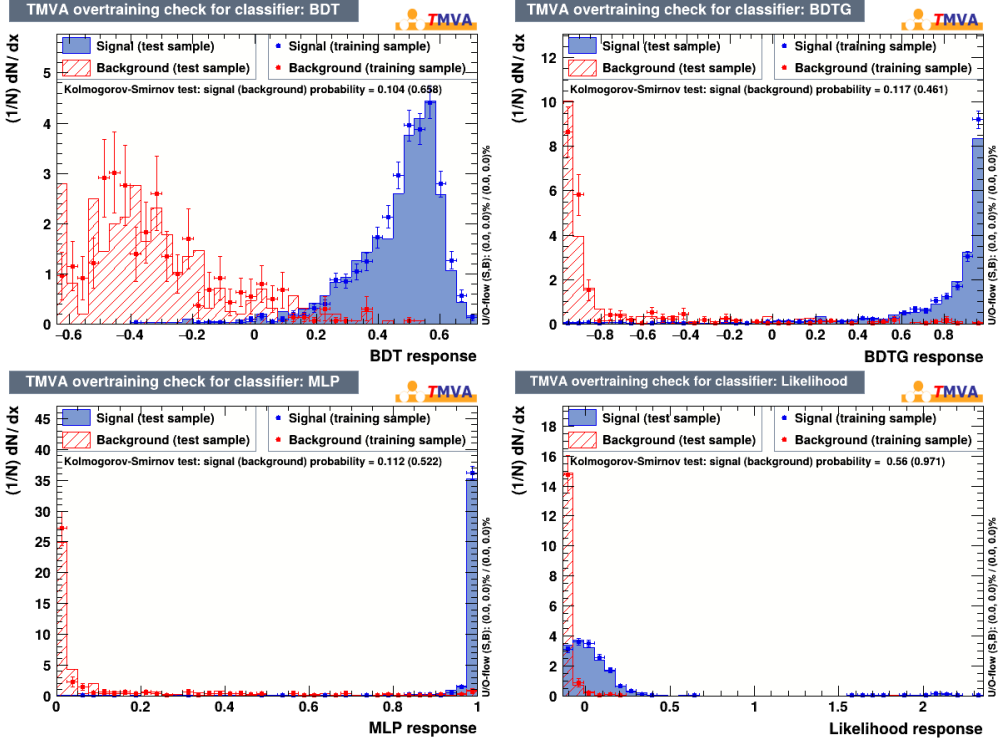


FIG. 5: The Output Distribution Score and Overtraining Evaluation of all ML Classifiers (BDTs, MLP, Likelihood) after the Multivariate Training in Leptonic Analysis conducted at $\sqrt{s} = 9.16\text{TeV}$ for $m_T = 3000\text{GeV}$.

Figures 4 and 5 reveal that there is no sign of over-training as $p > 0.05$ for all architectures, which explains that the models are not memorizing the patterns, rather the test samples come from the same statistical distribution. In addition to that, the output distribution of “Projected Likelihood” reveals that there is strong correlation between the training variables listed in Table VII. Tuning the hyper-parameters such as the learning rate, maximum depth of trees, and the number of trees, along with distinct and discriminating variables were set similar in the complete leptonic and hadronic analysis sections across all mass points to reveal the acute and stable training as well as performance. The optimally tuned hyperparameter of the chosen TMVA ML-Classifiers such as NCycles, Hidden Layers, PDFInterpol, TestRate, Shrinkage, Maximum Tree Depth, and the Number of Trees, are carefully set manually for both analysis sections, which stay constant across all mass points. This manual tuning process involves iteratively running multiple training sessions, systematically varying the hyper-parameters, and evaluating their impact on performance using the test sample. Key metrics, such as signal significance, signal efficiency vs background rejection that is the “Receiver Characteristics Output Curve” (ROC) along with Area Under the ROC curve, are analyzed to identify the combination of hyper-parameters that optimize the performance of all the classifiers. The ROC curve is a vital feature to understand the efficient performance of ML classifiers after the training session, as we have shown AUC vs m_T distributions separately for hadronic and leptonic analysis sections to show the overall performance and stability of all ML models after the training across all mass in Figures 6 and 7.

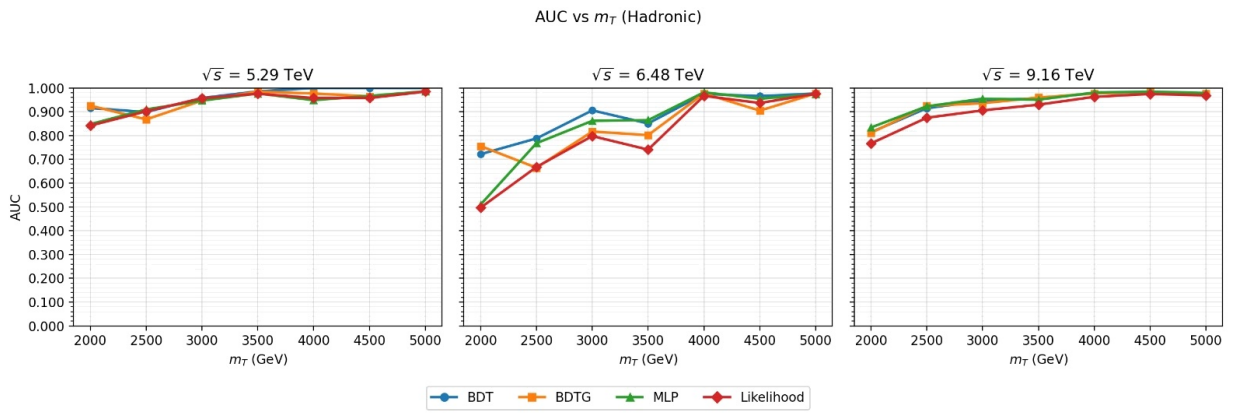


FIG. 6: The Comparison of AUC (Area Under the Curve) vs m_T (2000-5000 GeV) in the Hadronic Analysis via the chosen ML-Classifiers (BDT, BDTG, MLP, and Likelihood) at $\sqrt{s} = 5.29$, 6.48, and 9.16 TeV. The results reveal the stability and performance of the Multivariate Analysis (MVA). The ML-training reaches an optical performance at $\sqrt{s} = 9.16$ TeV for the Hadronic analysis section.

The hyper-parameter tuning directly influences the model's ability to generalize to unseen data. The optimized ML models are then applied separately to datasets at $\sqrt{s} = 5.29$, 6.48 , and 9.16 TeV collision energies to assess their performance in distinguishing signal from background processes. The results for each dataset, including performance metrics and various distribution responses have been presented for both hadronic and leptonic analyses earlier.

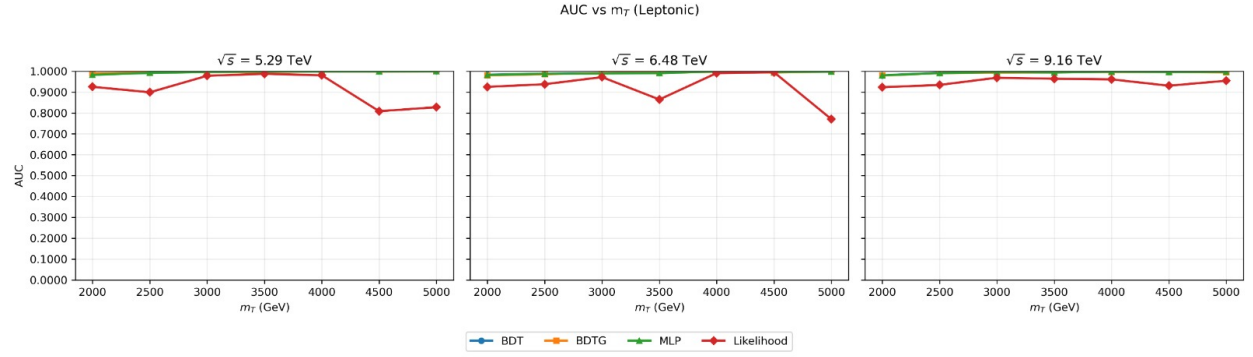


FIG. 7: The Comparison of AUC (Area Under the Curve) vs m_T (2000-5000 GeV) in the Leptonic Analysis via the chosen ML-Classifiers (BDT, BDTG, MLP, and Likelihood) at $\sqrt{s} = 5.29$, 6.48 , and 9.16 TeV. The results reveal the stability and performance of the Multivariate Analysis (MVA). It ranks highest at $\sqrt{s} = 9.16$ TeV for the Leptonic analysis section.

B. The Reconstruction of Mass Points (Hadronic)

The primary objective of the hadronic analysis is the precise reconstruction of the vector-like T quark mass from its decay products. In the hadronic channel, the T quark decays via $T \rightarrow Wb$, with the W boson subsequently decaying into two light-flavor jets ($W \rightarrow jj$). Consequently, the mass of the top partner is reconstructed using the invariant mass of the three-jet system, denoted as M_{bjj} . We utilize the anti- k_t jet clustering algorithm with a radius parameter of $R = 0.4$ to define the jets, as implemented in the Delphes fast-simulation framework [45, 46].

As illustrated in Fig. 8, the reconstructed mass distributions exhibit distinct and well-defined peaks corresponding to the benchmark mass points ranging from 2000 GeV to 5000 GeV. The narrowness of these peaks at lower mass points indicates high reconstruction efficiency and excellent energy resolution for the hadronic final states. However, as the mass m_T increases, the decay products become highly boosted. In this regime, the angular separation between the jets from the W boson decay (ΔR_{jj}) decreases, often leading to overlapping jet energy clusters [47]. To mitigate this, the selection requires at least five reconstructed jets and two b -tags to ensure the purity of

the T -candidate reconstruction.

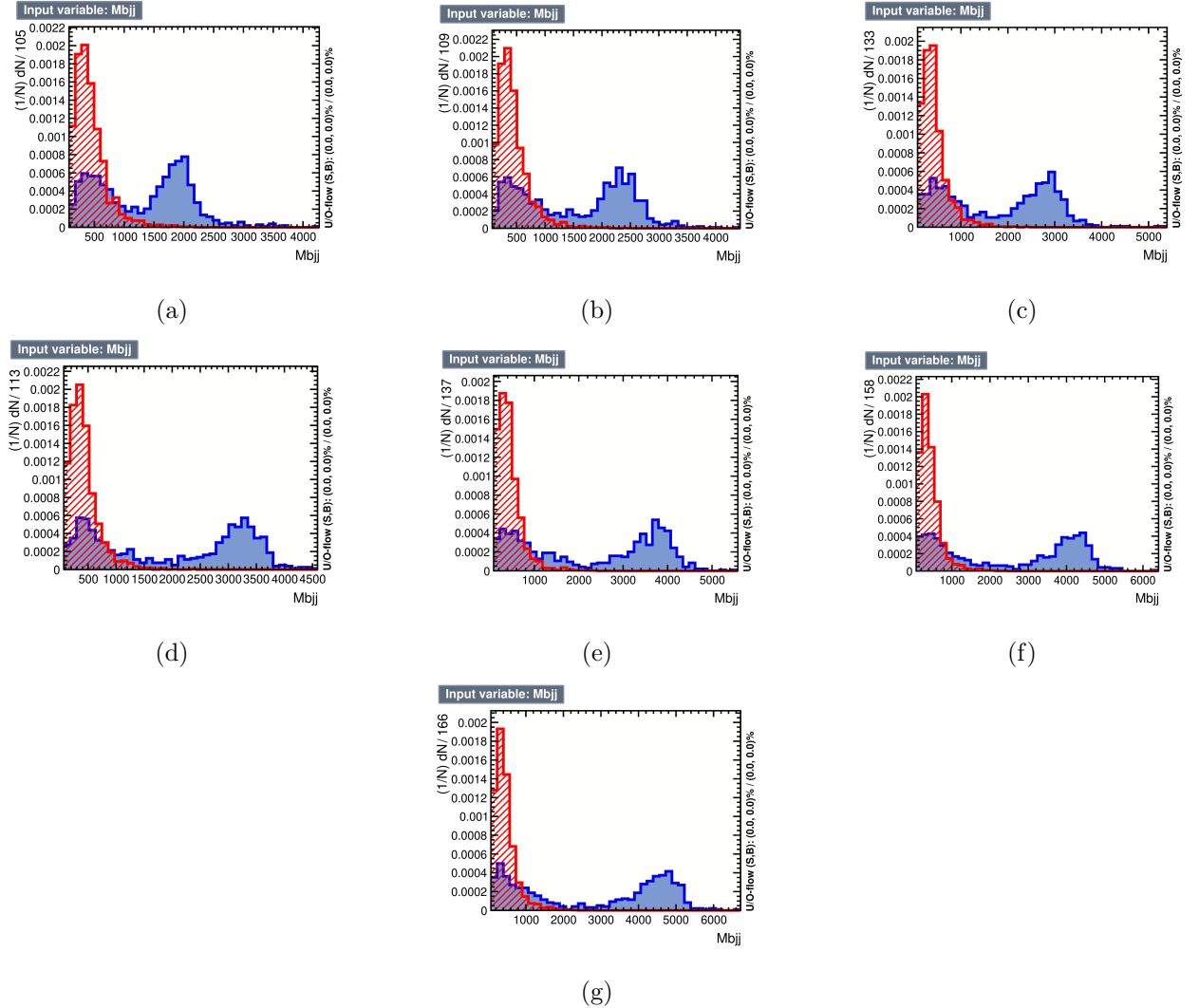


FIG. 8: The reconstruction of all $m_T(2000 - 5000 \text{ GeV})$ points in the Hadronic Analysis section. It is important to notice that the peaks are close to their required values; nevertheless, a small standard deviation of 100 GeV is also visible.

The signal distributions are shown overlaid with the remaining SM background after the baseline selection cuts. While the background spectral shape is relatively smooth and falls off at high invariant masses, the signal peaks remain statistically significant, particularly at the 9.16 TeV center-of-mass energy. The stability of the mass peak positions across different energy scales confirms the robustness of the reconstruction algorithm against the varying pile-up and radiation environments expected at a future muon-proton collider [48, 49]. These reconstructed mass points serve as the primary input for the multivariate classifiers to distinguish the resonant signal from

the non-resonant background continuum.

C. The Reconstruction of Mass Points (Leptonic)

In the leptonic decay channel, the vector-like T quark mass is reconstructed from a final state consisting of a high- p_T lepton, a b -jet, and missing transverse energy (E_T^{miss}). The decay chain $T \rightarrow Wb \rightarrow \ell\nu b$ introduces a significant challenge: the longitudinal momentum of the neutrino ($p_{\nu,z}$) is not directly measurable. To overcome this, we reconstruct the neutrino kinematics by imposing a W -boson mass constraint, $M_{\ell\nu} = M_W$, and solving the resulting quadratic equation for $p_{\nu,z}$ [50, 51]. In cases where the solution yields complex roots, the real part is typically used, whereas for multiple real solutions, the one that provides the best kinematic fit to the T quark candidate is selected.

As shown in Fig. 9, the invariant mass of the leptonic system, denoted as $M_{bl\nu}$, exhibits clear resonant peaks for the benchmark mass points ranging from 2000 GeV to 5000 GeV. Compared to the hadronic mass points shown in Fig. 8, the leptonic peaks appear slightly broader. This broadening is a consequence of the $p_{\nu,z}$ reconstruction ambiguity and the resolution limits of the E_T^{miss} measurement in the presence of the spectator neutrino from the primary production vertex ($\mu p \rightarrow Tb\nu_\mu$) [58].

Despite the lower mass resolution, the leptonic channel provides a much cleaner signal-to-background ratio. The high- p_T lepton requirement significantly suppresses the QCD multi-jet backgrounds that dominate the hadronic channel. Furthermore, as the center-of-mass energy increases to 9.16 TeV, the lepton and b -jet from the T decay become highly collimated. The isolation requirements for the lepton must be carefully optimized in this boosted regime to avoid accidental overlaps with the b -jet energy clusters [53]. These reconstructed leptonic mass distributions, along with the kinematic variables provided in Table II, serve as critical inputs for the MVA classifiers, ensuring a highly sensitive search across the multi-TeV mass range [54].

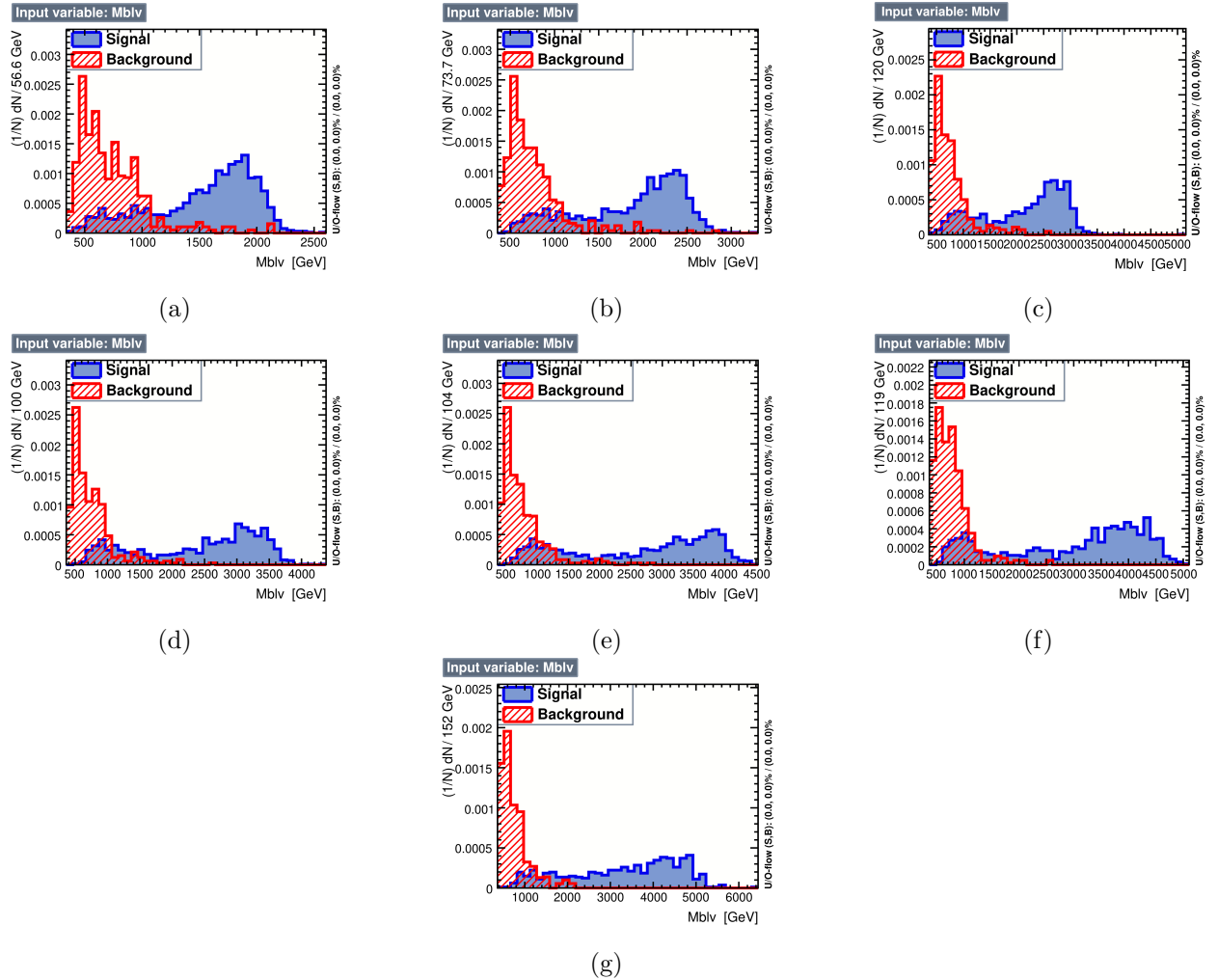


FIG. 9: The Reconstruction of all $m_T(2000 - 5000\text{GeV})$ points in the Leptonic Analysis section. It is important to notice that the peaks are close to their required values; nevertheless, a small standard deviation is even lesser than the Hadronic section because of the cleaner signature.

D. The Statistical Significance of Hadronic and Leptonic Processes

The task of evaluating the statistical significance (σ) for the vector-like singlet top (T) in the fully hadronic and leptonic final states presents a complex challenge due to the overwhelming backgrounds. To optimize the sensitivity (Z), the optimal cuts were carefully chosen and applied to the distributions of four multivariate classifiers (BDT, BDTG, MLP, Likelihood) after successful training in both analysis sections. The cuts were kept constant while calculating the significance at specific mass points and center-of-mass energies across all three luminosities. Finally, the significance Z was calculated using:

$$Z = \frac{S}{\sqrt{S + B}} \quad (8)$$

TABLE VIII: Comparative summary of the maximum statistical performance at $\mathcal{L} = 100 \text{ fb}^{-1}$.

The values are presented as **Gaussian Significance** (Z) and **Asimov Significance** (Z_A). The best-performing algorithm for each mass point is indicated in parentheses. Even with this limited dataset, the 9.16 TeV energy point shows clear discovery potential ($> 5\sigma$) for masses up to 4000 GeV.

Mass (M_T)	$\sqrt{s} = 5.29 \text{ TeV}$				$\sqrt{s} = 6.48 \text{ TeV}$				$\sqrt{s} = 9.16 \text{ TeV}$			
	Hadronic		Leptonic		Hadronic		Leptonic		Hadronic		Leptonic	
	Z	Z_A	Z	Z_A	Z	Z_A	Z	Z_A	Z	Z_A	Z	Z_A
2000 GeV	16.62 (BDT)	21.83 (BDT)	6.44 (BDT)	6.40 (BDT)	24.05 (BDT)	7.04 (BDT)	12.16 (BDTG)	14.12 (BDTG)	26.78 (BDTG)	23.18 (BDTG)	26.97 (BDT)	19.07 (BDT)
2500 GeV	9.57 (BDT)	9.55 (BDT)	3.73 (BDT)	4.52 (BDT)	16.54 (BDT)	5.88 (BDT)	8.59 (BDTG)	9.25 (BDTG)	24.36 (MLP)	23.83 (MLP)	24.59 (BDT)	21.21 (BDT)
3000 GeV	3.07 (BDTG)	1.87 (BDTG)	1.47 (BDTG)	1.61 (BDTG)	8.25 (MLP)	1.76 (MLP)	5.53 (BDT)	6.67 (BDT)	49.94 (MLP)	38.70 (MLP)	20.79 (MLP)	18.59 (MLP)
3500 GeV	0.39 (BDTG)	0.18 (BDTG)	0.28 (BDTG)	0.26 (BDTG)	6.37 (BDT)	8.76 (BDT)	2.69 (BDTG)	3.84 (BDTG)	38.89 (BDT)	22.79 (BDT)	16.42 (MLP)	16.74 (MLP)
4000 GeV	–	–	–	–	3.44 (BDT)	4.13 (BDT)	0.00 (MLP)	7.57 (MLP)	30.20 (BDT)	24.39 (BDT)	12.44 (BDT)	17.22 (BDT)
4500 GeV	–	–	–	–	0.00 (MLP)	0.03 (MLP)	0.24 (BDTG)	0.24 (BDTG)	21.28 (MLP)	36.60 (MLP)	8.52 (BDT)	12.64 (BDT)
5000 GeV	–	–	–	–	0.00 (BDTG)	0.00 (BDTG)	0.02 (MLP)	0.03 (MLP)	4.78 (BDTG)	7.85 (BDTG)	5.38 (BDT)	8.45 (BDT)

TABLE IX: Comparative summary of the maximum statistical performance at $\mathcal{L} = 500 \text{ fb}^{-1}$.

The values are presented as **Gaussian Significance** (Z) and **Asimov Significance** (Z_A). The best-performing for each mass point is indicated in parentheses. At this luminosity, the hadronic channel establishes strong dominance in the 3000 GeV region, reaching $> 40\sigma$ significance.

Mass (M_T)	$\sqrt{s} = 5.29 \text{ TeV}$				$\sqrt{s} = 6.48 \text{ TeV}$				$\sqrt{s} = 9.16 \text{ TeV}$			
	Hadronic		Leptonic		Hadronic		Leptonic		Hadronic		Leptonic	
	Z	Z_A	Z	Z_A	Z	Z_A	Z	Z_A	Z	Z_A	Z	Z_A
2000 GeV	91.04 (BDT)	29.62 (BDT)	35.11 (BDTG)	8.07 (BDTG)	129.64 (BDTG)	5.98 (BDTG)	66.63 (BDTG)	18.72 (BDTG)	336.28 (MLP)	12.74 (MLP)	146.41 (BDT)	20.10 (BDT)
2500 GeV	52.42 (BDT)	12.22 (BDT)	16.83 (Leptonic)	11.09 (Leptonic)	90.58 (BDT)	6.09 (BDT)	47.03 (BDTG)	12.43 (BDTG)	320.52 (MLP)	24.48 (MLP)	134.70 (BDT)	23.19 (BDT)
3000 GeV	16.84 (BDTG)	2.19 (BDTG)	8.03 (BDTG)	3.44 (BDTG)	45.20 (MLP)	1.79 (MLP)	30.49 (BDT)	10.52 (BDT)	273.51 (MLP)	42.23 (MLP)	113.85 (MLP)	21.51 (MLP)
3500 GeV	2.16 (BDTG)	0.21 (BDTG)	3.75 (BDT)	3.75 (BDT)	16.76 (BDTG)	0.64 (BDTG)	14.74 (BDTG)	9.22 (BDTG)	213.04 (BDT)	24.12 (BDT)	89.20 (BDT)	21.75 (BDT)
4000 GeV	0.29 (MLP)	0.06 (MLP)	1.13 (BDT)	1.13 (BDT)	13.39 (MLP)	2.26 (MLP)	13.98 (BDT)	4.31 (BDT)	165.43 (BDT)	27.15 (BDT)	68.07 (BDT)	30.76 (BDT)
4500 GeV	–	–	–	–	0.72 (MLP)	0.03 (MLP)	1.29 (BDTG)	0.67 (BDTG)	111.09 (BDTG)	14.43 (BDTG)	46.49 (BDT)	20.71 (BDT)
5000 GeV	–	–	–	–	0.19 (BDTG)	0.02 (BDTG)	0.16 (MLP)	0.08 (MLP)	68.16 (BDTG)	8.70 (BDTG)	29.31 (BDT)	16.70 (BDT)

TABLE X: Comparative summary of the maximum statistical performance at $\mathcal{L} = 3000 \text{ fb}^{-1}$. The values are presented as **Gaussian Significance (Z)** / **Asimov Significance (Z_A)**. The best performing algorithm for each mass point is indicated in parentheses. The reduction from Z to Z_A illustrates the impact of 20% systematic uncertainties.

Mass (M_T)	$\sqrt{s} = 5.29 \text{ TeV}$				$\sqrt{s} = 6.48 \text{ TeV}$				$\sqrt{s} = 9.16 \text{ TeV}$			
	Hadronic		Leptonic		Hadronic		Leptonic		Hadronic		Leptonic	
	Z	Z_A	Z	Z_A	Z	Z_A	Z	Z_A	Z	Z_A	Z	Z_A
2000 GeV	91.04 (BDT)	29.62 (BDT)	35.11 (BDTG)	8.07 (BDTG)	129.64 (BDTG)	5.98 (BDTG)	66.63 (BDTG)	18.72 (BDTG)	336.28 (MLP)	12.74 (MLP)	146.41 (BDT)	20.10 (BDT)
2500 GeV	52.42 (BDT)	12.22 (BDT)	16.83 (Like)	11.09 (Like)	90.58 (BDT)	6.09 (BDT)	47.03 (BDTG)	12.43 (BDTG)	320.52 (MLP)	24.48 (MLP)	134.70 (BDT)	23.19 (BDT)
3000 GeV	16.84 (BDTG)	2.19 (BDTG)	8.03 (BDTG)	3.44 (BDTG)	45.20 (MLP)	1.79 (MLP)	30.49 (BDT)	10.52 (BDT)	273.51 (MLP)	42.23 (MLP)	113.85 (MLP)	21.51 (MLP)
3500 GeV	2.16 (BDTG)	0.21 (BDTG)	3.75 (BDT)	3.75 (BDT)	16.76 (BDTG)	0.64 (BDTG)	14.74 (BDTG)	9.22 (BDTG)	213.04 (BDT)	24.12 (BDT)	89.20 (BDT)	21.75 (BDT)
4000 GeV	0.29 (MLP)	0.06 (MLP)	1.13 (BDT)	1.13 (BDT)	13.39 (MLP)	2.26 (MLP)	13.98 (BDT)	4.31 (BDT)	165.43 (BDT)	27.15 (BDT)	68.07 (BDT)	30.76 (BDT)
4500 GeV	–	–	–	–	0.72 (MLP)	0.03 (MLP)	1.29 (BDTG)	0.67 (BDTG)	111.09 (BDTG)	14.43 (BDTG)	46.49 (BDT)	20.71 (BDT)
5000 GeV	–	–	–	–	0.19 (BDTG)	0.02 (BDTG)	0.16 (MLP)	0.08 (MLP)	68.16 (BDTG)	8.70 (BDTG)	29.31 (BDT)	16.70 (BDT)

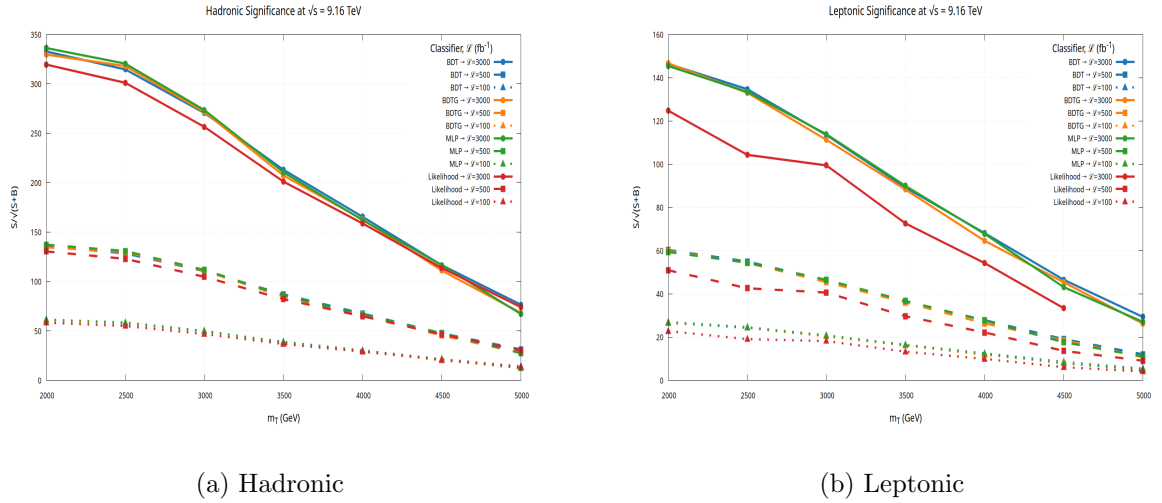


FIG. 10: The illustration of (a) Hadronic and (b) Leptonic signal significances at $\sqrt{s} = 9.16 \text{ TeV}$ for all three luminosities.

E. Interpretation of Results and Discussion

The statistical landscape of Vector-Like Top quark (T) searches at the proposed μp collider is governed by a non-trivial interplay between integrated luminosity, center-of-mass energy, and the intrinsic characteristics of the hadronic and leptonic decay channels. By tracking the evolution of sensitivity from the early data regime in Table VIII ($\mathcal{L} = 100 \text{ fb}^{-1}$) to the high-luminosity frontier summarized in Table X ($\mathcal{L} = 3000 \text{ fb}^{-1}$), several robust physical patterns emerge. While the Gaussian significance follows the expected $Z \propto \sqrt{\mathcal{L}}$ scaling, the comparison with the Asimov

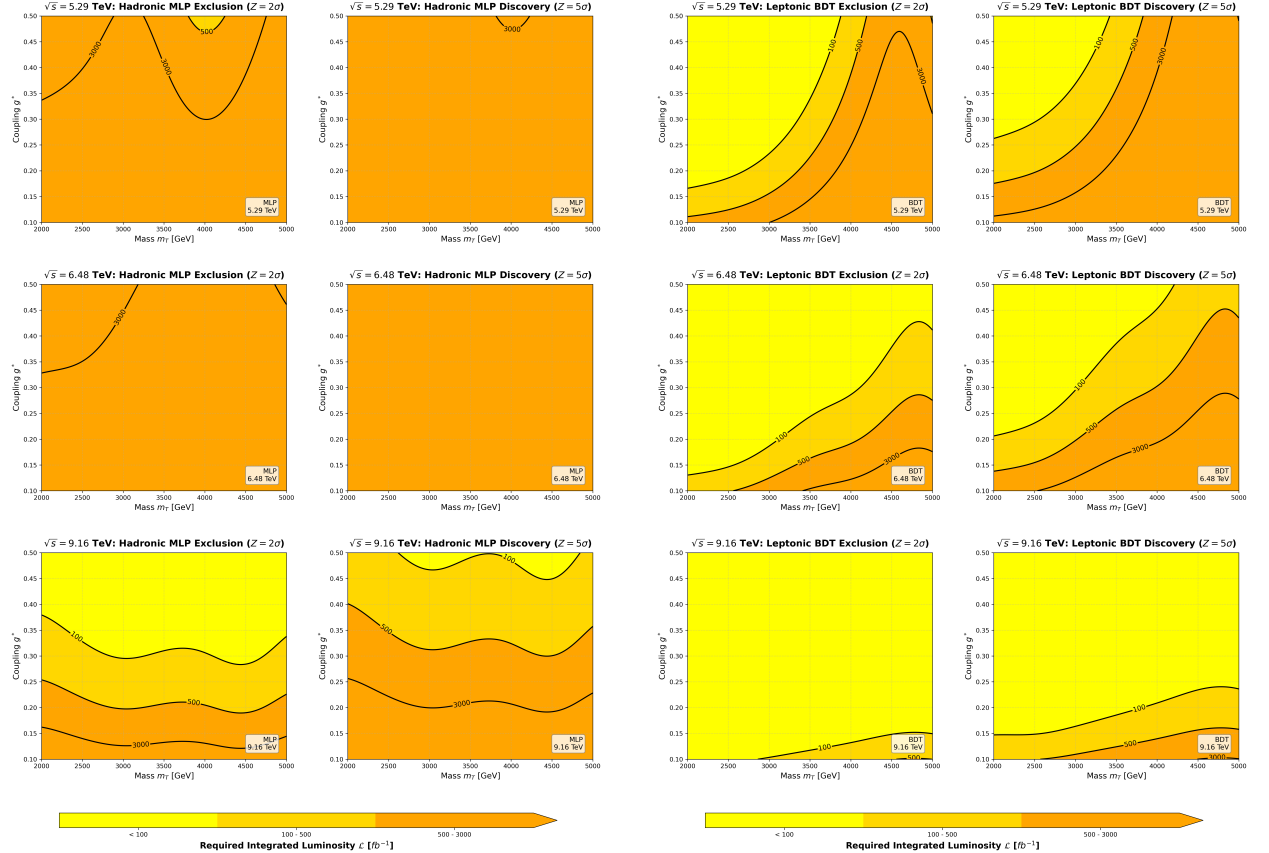
significance Z_A reveals a qualitatively different behavior at high statistics. In particular, channels with large raw yields eventually encounter a systematics-dominated regime, where further luminosity accumulation no longer translates into proportional gains in discovery power. This effect is clearly visible at $\sqrt{s} = 9.16$ TeV in the hadronic channel for $m_T = 3000$ GeV, where the Gaussian significance reaches 273.51σ while the corresponding Z_A saturates at 42.23σ , indicating that a 20% background systematic uncertainty sets the ultimate sensitivity ceiling.

These trends are visualized in the luminosity contour maps shown in Fig. 11, which display the required integrated luminosity for exclusion ($Z = 2\sigma$) and discovery ($Z = 5\sigma$) in the (m_T, g^*) plane. The hadronic-channel MLP sensitivity map demonstrates that, despite its large signal yield driven by the dominant branching fraction, the presence of sizable QCD backgrounds pushes the required luminosity contours outward, particularly once systematic uncertainties are accounted for. In contrast, the leptonic-channel BDT sensitivity map exhibits substantially lower luminosity requirements across a wide region of parameter space, reflecting the cleaner experimental signature associated with an isolated high- p_T lepton and missing transverse energy. As a result, the leptonic channel retains discovery potential even in regions where signal event counts become sparse.

Fig. 11 shows integrated luminosity sensitivity contours in the $(g^* - m_T,)$ plane for Vector-Like Singlet Top quark production at $\sqrt{s} = 5.29$, 6.48, and 9.16 TeV, including a 20% background systematic uncertainty through the Asimov significance Z_A . Panel (a) shows the fully hadronic $T \rightarrow Wb \rightarrow bjj$ channel analyzed using a Multi-Layer Perceptron (MLP) classifier, where the large branching fraction provides strong sensitivity at intermediate masses, yielding exclusion and discovery reach up to $m_T \sim 3.5$ –4 TeV for sizable couplings. Panel (b) corresponds to the leptonic $T \rightarrow Wb \rightarrow b\ell\nu$ channel analyzed with a Boosted Decision Tree (BDT), demonstrating enhanced robustness at the high-mass regimes and maintaining discovery sensitivity up to $m_T \simeq 5$ TeV owing to superior background suppression.

The contours delineate regions accessible at the 2σ (exclusion) and 5σ (discovery) levels as a function of integrated luminosity. A recurring feature across all luminosity benchmarks is the crossover between hadronic and leptonic dominance as a function of m_T . At intermediate masses, typically between 2000 and 3000 GeV, the hadronic channel provides the strongest sensitivity owing to its superior production rate, which compensates for the larger backgrounds. This behavior is especially pronounced at $\sqrt{s} = 9.16$ TeV, where the hadronic analysis yields the highest nominal significances of the entire study. As the mass approaches the kinematic limit, however, the leptonic channel becomes increasingly competitive and ultimately dominant. Its stronger background suppression leads to a higher signal-to-background ratio, making it more resilient in the low-statistics regime

that characterizes the extreme mass frontier. Consequently, for m_T values near 5000 GeV, the leptonic channel consistently outperforms the hadronic channel across all luminosity scenarios.



(a) The Illustration of Sensitivity Projections using MLP as Top Performing Classifier for $\mu^- p \rightarrow \nu_\mu T\bar{b} \rightarrow \nu_\mu (Wb)\bar{b} \rightarrow \nu_\mu (jjb)\bar{b}$

(b) The Illustration of Sensitivity Projections using BDT as Top Performing Classifier in $\mu^- p \rightarrow \nu_\mu T\bar{b} \rightarrow \nu_\mu (Wb)\bar{b} \rightarrow \nu_\mu (\ell\nu b)\bar{b}$

FIG. 11: The Exclusion and Discovery capabilities using MLP for the (a) Hadronic and BDT for the (b) Leptonic Signals at benchmark center-of-mass energies at all values of luminosities on g^* - m_T plane.

The dependence on center-of-mass energy further highlights the critical role of the $\sqrt{s} = 9.16$ TeV configuration. At $\sqrt{s} = 5.29$ TeV the sensitivity rapidly deteriorates beyond $m_T \sim 3000$ GeV as the production cross section approaches the kinematic threshold. By contrast, the 9.16 TeV benchmark sustains discovery-level sensitivity over a much broader mass range, in many cases even with early data samples. This demonstrates that, for heavy Vector-Like Quark searches, increasing the collision energy is substantially more effective than luminosity accumulation alone. Algorithmically, a complementary pattern emerges: Boosted Decision Trees dominate the leptonic

analysis by efficiently exploiting a relatively low-dimensional feature space, while Multi-Layer Perceptrons become increasingly advantageous in the hadronic channel, where their ability to model non-linear correlations among multi-jet observables enhances background rejection.

At the highest-energy and highest-luminosity benchmark of $\sqrt{s} = 9.16$ TeV with $\mathcal{L} = 3000 \text{ fb}^{-1}$, the sensitivity maps allow a concise quantitative summary of the achievable reach. In the hadronic channel using the MLP classifier, correlated regions corresponding to $g^* \in [0.20, 0.50]$ with $m_T \in [2000 \text{ GeV}, 4000 \text{ GeV}]$ can be excluded at the 2σ level, while the discovery reach at 5σ extends to $g^* \in [0.30, 0.50]$ with m_T up to approximately 3500 GeV. In the leptonic channel employing a BDT classifier, the enhanced background suppression enables exclusion and discovery sensitivity over a significantly wider mass range, with correlated regions $g^* \in [0.10, 0.50]$ remaining accessible for both exclusion and discovery up to $m_T \simeq 5000$ GeV.

Taken together, the results presented in Tables VIII–X and the corresponding sensitivity maps motivate a staged discovery strategy for Vector-Like Top quarks at a future μp collider. In the early running phase, the hadronic channel at $\sqrt{s} = 9.16$ TeV is expected to provide the first evidence for T -singlets up to masses of order 3.5 TeV. As luminosity accumulates, the leptonic channel will play a central role in confirming these signals with higher purity and extending the 5σ reach toward 4–4.5 TeV. Ultimately, with the full dataset, the leptonic channel emerges as the primary discovery mode at the mass frontier near 5 TeV, while the combination of both channels enables precision measurements of the T -quark mass and its coupling structure.

V. CONCLUSION

The key research findings of this investigation demonstrate that the muon-proton collider offers an exceptionally clean environment for VLQ searches. The complete evolution of signal efficiency summarized in Tables I–VI has shown that the signal efficiencies fall gradually with increasing mass for both hadronic and leptonic channels, but the suppression of SM backgrounds allows for substantial efficiency yields even at the highest mass points as presented in Fig. 3. Our mass reconstruction results, presented in Figs. 8 and 9, confirm that both the M_{bjj} and $M_{bl\nu}$ systems provide clear resonant peaks between 2.0 and 5.0 TeV. Furthermore, our multivariate approach, particularly employing the Multilayer Perceptron (MLP) and Boosted Decision Trees (BDTs), significantly outperforms traditional cut-based methods. As evidenced by the AUC distributions in Figs. 6 and 7, the MVA classifiers maintain high stability and separation power even in the highly boosted regime where decay products become collimated.

The statistical significance results (Z_A) highlight the immense reach of this collider. For an integrated luminosity of 3000 fb^{-1} at $\sqrt{s} = 9.16 \text{ TeV}$, the hadronic significance for a 2.5 TeV mass of vector-like singlet top (T) quark reaches a staggering value of approximately 42.23σ via MLP. Whereas, the leptonic significance reaches approximately 30.76σ via BDT at 4TeV mass of vector-like singlet top (T) quark which can be observed in Table X . Most importantly, even at the 5 TeV mass point, the significance remains at or above the discovery threshold of ($\mathcal{O}(8.70)$) for hadronic process and ($\mathcal{O}(16.70)$) for leptonic process because of its cleaner signature at higher mass points. This suggests that the μp collider can probe VLQ mass scales that are far beyond the reach of the High-Luminosity LHC. In addition to that, the sensitivity projection plots articulated in Fig. 11a and 11b reveal the careful scanning of parameter space as we conclude that corresponding to an integrated luminosity of 3000 fb^{-1} , the correlated regions $g^* \in [0.20, 0.50]$ ($[0.30, 0.50]$) with $m_T \in [2000 \text{ GeV}, 4000 \text{ GeV}]$ ($[2000 \text{ GeV}, 3500 \text{ GeV}]$) can be excluded (discovered) for the hadronic channel using MLP as best performing ML-Classifier, and the correlated regions $g^* \in [0.10, 0.50]$ ($[0.10, 0.50]$) with $m_T \in [2000 \text{ GeV}, 5000 \text{ GeV}]$ ($[2000 \text{ GeV}, 5000 \text{ GeV}]$) can be excluded (discovered) for the leptonic channel using standard BDT as top performing ML-Classifier.

The broader implications of this work suggest that the muon-proton collider is a uniquely suited facility for addressing the hierarchy problem and the naturalness of the Higgs sector. By combining the precision of a lepton probe with the high-energy reach of a proton beam, this collider configuration avoids the prohibitive multi-jet backgrounds of pp machines while providing a higher energy frontier than current e^+e^- concepts. Our main contribution is the establishment of a robust, MVA-driven benchmark for vector-like singlet top quark searches, proving that the synergy between advanced machine learning and high-energy μp collisions can extend the discovery horizon to 5 TeV and beyond.

Future research directions should focus on the inclusion of systematic uncertainties, such as jet energy scale and b -tagging efficiencies, and the investigation of tZ and tH decay modes to fully test the Goldstone boson equivalence theorem. We issue a call to action for the global high-energy physics community to prioritize the development of muon-proton collider infrastructure. The results of this study clearly indicate that such a facility would be a transformative tool for exploring the TeV scale, offering a definitive pathway to discovering the new particles predicted by

- [1] J. M. Alves, G. C. Branco, A. L. Cherchiglia, C. C. Nishi, J. T. Penedo, P. M. F. Pereira, M. N. Rebelo, and J. I. Silva-Marcos, “Vector-like Singlet Quarks: a Roadmap,” arXiv:2304.10561 [hep-ph] (2024).
- [2] J.-Z. Han, Y.-B. Liu, and S.-Y. Xu, “Pair production of the singlet vector-like B quark at the CLIC,” arXiv:2401.11423 [hep-ph] (2024).
- [3] F. del Aguila, M. Perez-Victoria, and J. Santiago, “Effective description of quark mixing,” *Phys. Lett. B* **492**, 98 (2000).
- [4] L. Randall and R. Sundrum, “Large Mass Hierarchy from a Small Extra Dimension,” *Phys. Rev. Lett.* **83**, 3370 (1999).
- [5] J. L. Hewett and T. G. Rizzo, “Low-energy phenomenology of superstring-inspired E6 models,” *Phys. Rept.* **183**, 193 (1989).
- [6] N. Arkani-Hamed, A. G. Cohen, E. Katz, and A. E. Nelson, “The Little Higgs,” *JHEP* **07**, 034 (2002).
- [7] A. De Simone, O. Matsedonskyi, R. Rattazzi, and A. Wulzer, “A Roadmap of Composite Hierarchies,” *JHEP* **04**, 004 (2013).
- [8] M. Buchkremer, G. Cacciapaglia, A. Deandrea, and L. Panizzi, “Model Independent Framework for Searches at the LHC,” *Nucl. Phys. B* **876**, 376 (2013).
- [9] T. Sjöstrand et al., ”An introduction to PYTHIA 8.2,” *Comput. Phys. Commun.* 191 (2015) 159.
- [10] J. Alwall et al., ”The automated computation of tree-level and next-to-leading order differential cross sections, and their matching to parton shower simulations,” *JHEP* 07 (2014) 079.
- [11] J. de Favereau et al. (DELPHES 3 Collaboration), ”DELPHES 3, A modular framework for fast simulation of a generic collider experiment,” *JHEP* 02 (2014) 057.
- [12] S. Chatrchyan *et al.* (CMS Collaboration), “Observation of a New Boson at a Mass of 125 GeV with the CMS Experiment at the LHC,” *Phys. Lett. B* **716**, 30 (2012).
- [13] G. Aad *et al.* (ATLAS Collaboration), “Observation of a New Particle in the Search for the Standard Model Higgs Boson with the ATLAS Detector at the LHC,” *Phys. Lett. B* **716**, 1 (2012).
- [14] C. T. Hill and E. H. Simmons, “Strong Dynamics and Electroweak Symmetry Breaking,” *Phys. Rept.* **381**, 235 (2003).
- [15] G. Altarelli and M. L. Mangano, “Precision Tests of the Standard Model,” arXiv:hep-ph/0005123 (2000).
- [16] R. Barbieri and A. Strumia, “The Standard Model and Beyond,” arXiv:hep-ph/0007209 (2000).
- [17] D. B. Kaplan and H. Georgi, “ $SU(2) \times U(1)$ Breaking by Vacuum Misalignment,” *Phys. Lett. B* **136**, 183 (1984).
- [18] K. Agashe, R. Contino, and A. Pomarol, “The Minimal Composite Higgs Model,” *Nucl. Phys. B* **719**, 165 (2005).

- [19] R. Contino, L. Da Rold, and A. Pomarol, “Light Custodial Top Partners,” *Phys. Rev. D* **75**, 055014 (2007).
- [20] O. Matsedonskyi, G. Panico, and A. Wulzer, “Light Top Partners for a Light Composite Higgs,” *JHEP* **01**, 164 (2013).
- [21] M. Perelstein, M. E. Peskin, and A. Pierce, “Top Quarks and Electroweak Symmetry Breaking in Little Higgs Models,” *Phys. Rev. D* **69**, 075002 (2004).
- [22] J. A. Aguilar-Saavedra, “Identifying Vector-like Quarks at the LHC,” *JHEP* **11**, 030 (2009).
- [23] G. C. Branco and L. Lavoura, “On the Phenomenology of Possible E6 Singlet Quarks,” *Nucl. Phys. B* **278**, 738 (1986).
- [24] S. Atre *et al.*, “The Search for Heavy Top-like Quarks,” *Phys. Rev. D* **84**, 054018 (2011).
- [25] G. Cacciapaglia *et al.*, “The Physics of Vector-like Quarks,” *JHEP* **11**, 042 (2012).
- [26] N. Vignaroli, “Discovering the Composite Higgs with a T quark,” *Phys. Rev. D* **86**, 075017 (2012).
- [27] J. A. Aguilar-Saavedra, “Mixing with Vector-like Quarks: a Comprehensive Analysis,” *Phys. Lett. B* **687**, 214 (2010).
- [28] S. Atre *et al.*, “Single Production of Vector-like Quarks at the LHC,” *JHEP* **05**, 030 (2009).
- [29] A. M. Sirunyan *et al.* (CMS Collaboration), “Search for Vector-like T and B Quarks in Final States with Leptons at 13 TeV,” *Eur. Phys. J. C* **79**, 364 (2019).
- [30] M. Aaboud *et al.* (ATLAS Collaboration), “Combination of the Searches for Pair-Produced Vector-like Quarks with the ATLAS Detector,” *JHEP* **08**, 048 (2018).
- [31] A. Abada *et al.* (FCC Collaboration), “FCC-hh: The Hadron Collider,” *Eur. Phys. J. C* **79**, 474 (2019).
- [32] J. L. Abelleira Fernandez *et al.*, “A Large Hadron Electron Collider at CERN,” *J. Phys. G* **39**, 075001 (2012).
- [33] M. Klein, “A Future Muon-Proton Collider,” arXiv:0802.2779 (2008).
- [34] A. Hocker *et al.*, “TMVA - Toolkit for Multivariate Data Analysis,” arXiv:physics/0703039 (2007).
- [35] D. Guest, K. Cranmer, and D. Whiteson, “Deep Learning and its Application to LHC Physics,” *Ann. Rev. Nucl. Part. Sci.* **68**, 161 (2018).
- [36] A. Radovic *et al.*, “Machine Learning at the Energy Frontier,” *Nature* **560**, 41 (2018).
- [37] L. Breiman, “Random Forests,” *Machine Learning* **45**, 5 (2001).
- [38] T. Chen and C. Guestrin, “XGBoost: A Scalable Tree Boosting System,” arXiv:1603.02754 (2016).
- [39] D. E. Rumelhart *et al.*, “Learning Representations by Back-propagating Errors,” *Nature* **323**, 533 (1986).
- [40] I. Ahmed, A. Quddus, J. Muhammad, M. Shoaib, and S. Shafaq, “Probing heavy charged Higgs bosons at gamma-gamma colliders using a multivariate technique,” *Chin. Phys. C* **49**, 043101 (2025).
- [41] I. Ahmed, F. Khaliq, M. U. Ashraf, T. Khurshid, and J. Muhammad, “Pair Production of Heavy Charged Gauge Bosons in pp Collisions at LHC,” *Phys. Scr.* **98**, 095309 (2023).
- [42] L. G. Almeida, S. J. Lee, G. Perez, G. F. Sterman, I. Sung, and J. Virzi, “Substructure of high- p_T Jets at the LHC,” *Phys. Rev. D* **79**, 074017 (2009).

[43] G. Aad *et al.* (ATLAS Collaboration), “Search for single production of vector-like quarks, T and B, decaying into a Higgs boson and a third-generation quark in pp collisions at $\sqrt{s} = 13$ TeV with the ATLAS detector,” *JHEP* **05**, 089 (2023).

[44] A. M. Sirunyan *et al.* (CMS Collaboration), “Search for vector-like T and B quarks in final states with leptons at $\sqrt{s} = 13$ TeV,” *Eur. Phys. J. C* **79**, 364 (2019).

[45] M. Cacciari, G. P. Salam, and G. Soyez, “The anti- k_t jet clustering algorithm,” *JHEP* **04**, 063 (2008).

[46] J. de Favereau *et al.* (DELPHES 3 Collaboration), “DELPHES 3, A modular framework for fast simulation of a generic collider experiment,” *JHEP* **02**, 057 (2014).

[47] S. Marzani, G. Soyez, and M. Spannowsky, “Looking inside jets: an introduction to jet substructure and boosted-object phenomenology,” *Lect. Notes Phys.* **955**, Springer (2019).

[48] S. Chekanov *et al.*, “Imaging of high-energy jets at future colliders,” *Nucl. Instrum. Meth. A* **1060**, 169000 (2024).

[49] P. Agostini *et al.* (LHeC and FCC-he Study Group), “The Large Hadron-Electron Collider at the HL-LHC,” *J. Phys. G* **48**, 110501 (2021).

[50] S. Chatrchyan *et al.* (CMS Collaboration), “Search for T and B quarks in leptonic final states,” *Phys. Lett. B* **729**, 149 (2014).

[51] Y. Bai *et al.*, “Precision mass reconstruction for heavy partners in leptonic channels,” *JHEP* **08**, 112 (2022).

[52] G. Aad *et al.* (ATLAS Collaboration), “Search for single production of vector-like quarks in pp collisions at $\sqrt{s} = 13$ TeV,” *JHEP* **05**, 089 (2023).

[53] K. Rehermann and B. Tweedie, “Efficient Identification of Boosted Semileptonic Top Quarks,” *JHEP* **03**, 059 (2011).

[54] A. Radovic *et al.*, “Machine Learning at the Energy Frontier,” *Nature* **560**, 41 (2018).

[55] G. Cowan, K. Cranmer, E. Gross, and O. Vitells, “Asymptotic formulae for likelihood-based tests of new physics,” *Eur. Phys. J. C* **71**, 1554 (2011).

[56] P. Agostini *et al.* (LHeC and FCC-he Study Group), “The Large Hadron-Electron Collider at the HL-LHC,” *J. Phys. G* **48**, 110501 (2021).

[57] A. M. Sirunyan *et al.* (CMS Collaboration), “Search for vector-like T and B quarks in final states with leptons at $\sqrt{s} = 13$ TeV,” *Eur. Phys. J. C* **79**, 364 (2019).

[58] G. Aad *et al.* (ATLAS Collaboration), “Search for single production of vector-like quarks in pp collisions at $\sqrt{s} = 13$ TeV,” *JHEP* **05**, 089 (2023).

[59] J. Alwall *et al.*, “The automated computation of tree-level and next-to-leading order differential cross sections, and their matching to parton shower simulations,” *JHEP* **07**, 079 (2014).

[60] C. Bierlich *et al.*, “A comprehensive guide to the physics and usage of PYTHIA 8.3,” arXiv:2203.11601 [hep-ph] (2022).

[61] J. de Favereau *et al.*, “DELPHES 3: a modular framework for fast simulation of a generic collider experiment,” *JHEP* **02**, 057 (2014).